Thermal Emission Hot-Spot Effect of Crop Canopies—Part I: Simulation

Huaguo Huang, Qinhuo Liu, and Wenhan Qin

***Abstract*—This paper is the first part of a three-part article series. Simulations of directional brightness temperature over both simple canopies with triangular leaves and the row-planted wheat and corn were used to analyze the thermal emission hot-spot effect on crop canopies. Two models, *Cupid* and *TRGM*, were successively used to simulate the thermal hot-spot signatures under conditions which cannot be easily captured in reality. The investigation includes the planting row structure, the leaf area index (LAI), the leaf angle distribution (LAD), the component temperature distribution as well as variations in the microclimate. The results show that there are typically three types of directional emission shapes in the solar principle plane: the bowl, dome and bell shape. Regardless of the shape, the hot spot is significant and can be accurately fitted ($\mathrm{R}^2 = 0.98$ and $\mathrm{RMSE} = 0.04\,^{\circ}\mathrm{C}$) with a function of the phase angle (ξ), the hot-spot amplitude (ΔT_{HS}) and the half width of the hot spot (ξ_0), which can be quantified with the half width in the RED band. The planting row structure can reduce the ΔT_{HS} by a maximum amount (about 1.2 °C) when compared with an unstructured horizontal canopy. The ΔT_{HS} is linearly related to the component temperature differences between sunlit and shadowed parts. The linear equation can be used to predict the component temperature differences from ΔT_{HS}. The accuracy is very good for the horizontal canopies with triangular leaves ($\mathrm{RMSE} < 0.4\,^{\circ}\mathrm{C}$ and $R^2 > 0.99$), and acceptable for the virtual wheat and corn canopies ($\mathrm{RMSE} < 1.8\,^{\circ}\mathrm{C}$ and $R^2 > 0.81$).**

***Index Terms*—Component temperature difference, crop canopy, thermal emission directionality, thermal hot spot.**

I. Introduction

THE angular view effect is generally observed in the visible and near-infrared range (VNIR) as well as in the thermal infrared range (TIR). This effect can be described by the bidirectional reflectance distribution function (BRDF) in VNIR and is usually known as the thermal emission directionality in TIR. In VNIR, the hot-spot phenomenon is one of the most important features of BRDF. It describes a sharp peak of reflectance when the view direction coincides with the solar direction. The peak has a narrow width, which is highly related with vegetation structural parameters. For this reason, it has been used to estimate canopy structural parameters [1]. In TIR, a peak similar to that in VNIR should be observed when the view direction coincides with the solar direction [2]–[7]. To avoid confusion, we name the phenomenon in TIR the "thermal emission hot-spot effect."

The shadow-hiding mechanism [8], [9] has been the primary physical process accepted to explain the hot-spot effect for vegetation canopies both in laboratory experiments [9] and spaceborne measurements [10]. This mechanism occurs when the size of the individual scatterers is large compared with the wavelength, and thus well-defined shadows appear. These shadows are normally visible. However, they are invisible by the leaves or soil particles that cast them when the sun is right behind the observer, thus enhancing the reflectance in the backscattering. In the shadow-hiding theory, the half width is expected to be independent of wavelength.

Based on the shadow-hiding mechanism, many hot-spot models have been developed in order to incorporate this effect into canopy reflectance models [11], [12]. These models point to the potential of the hot-spot measurements from remote sensing applications to derive canopy architecture, including the leaf area index (LAI), leaf dimensions, and the leaf angle distribution (LAD). Further, Bréon *et al.* point out that the hot-spot amplitude is related to leaf reflectance [10]. Hence, for land surfaces studies, the main interest of measuring hot-spot signatures relies on its potential to retrieve leaf reflectance from the hot-spot amplitude and canopy structure from the hot-spot width.

Compared with the numerous studies of the hot-spot phenomenon in VNIR, the thermal emission hot-spot effect has received scant attention. The shadow of the instrument makes the laboratory and field measurements of the hot spot rather difficult. For this reason, Smith and Ballard were among the first who performed theoretical calculations of TIR hot spot over a homogeneous canopy using a 3-D vegetation model [13]. For simple homogeneous canopies, they predicted canopy TIR hot-spot variations of 2 °C at the surface with respect to nadir viewing. Similar to VNIR, the dependence of hot-spot width on leaf size is weak as long as the ratio of leaf size to canopy height is maintained and the angular width of the hot spot increases as the ratio of leaf diameter to canopy height increases. Atmospheric effects

Manuscript received June 17, 2009; revised October 25, 2009 and February 03, 2010; accepted March 16, 2010. Date of publication April 29, 2010; date of current version August 25, 2010. This work was supported in part by the Chinese Natural Science Foundation Project 40801135, the Chinese State Key Basic Research Project 2007CB714402, the Innovation Project of Beijing Forestry University under Contract BLYX200917, the Chinese Natural Science Foundation Project 40730525, the Research Fund for the Doctoral Program of Higher Education, the Chinese State Key Basic Research Project "Synthetic Retrieval of Territorial Ecological Variables Using both Active and Passive Remote Sensing Approaches" under Grant 2007CB714400, and the "WATER: Watershed Airborne Telemetry Experiment Research" under Grant KZCX2-XB2-09 under the auspices of the Chinese Academy of Sciences Action Plan for West Development Program.

H. Huang is with the Key Laboratory for Silviculture and Conservation of Ministry of Education, Beijing Forestry University, Beijing 100083, China (e-mail: huaguo.huang@gmail.com).

Q. Liu is with the State Key Laboratory of Remote Sensing Science, Beijing 100101, China.

W. Qin is with the NASA Goddard Space Flight Center, Greenbelt, MD 20771 USA, and also with the State Key Laboratory of Remote Sensing Science, Beijing 100101, China.

Digital Object Identifier 10.1109/JSTARS.2010.2046625

reduce but do not eliminate the TIR hot spot observed by satellites. Lagouarde *et al.* proposed a method of airborne experiments and measured the emission hot-spot effect of pine stands which shows significant hot-spot variations (2 °C–5 °C) in the solar principal plane (SPP) [5].

Until now, there has been no thorough analysis dealing with thermal emission hot-spot effect, not to mention the use of this information. Chen *et al.* conclude that the hot-spot effect is more complex than that in VNIR because of the complexity of energy balance processes [14]. For example, with 55° sun zenith angle, the maximum value of the emission radiation can appear at the nadir and not at the solar direction [7]. Therefore, it is necessary to make use of the special features of the thermal emission hot-spot effect and determine some useful information to derive the canopy architecture or component temperature distribution.

The objective of this paper is to quantitatively define the emission hot-spot effect and explore the potential to derive the information of component temperature distribution. Simulations of directional brightness temperature over simple canopies with triangular leaves, as well as the row-planted wheat and corn, will be used to analyze the thermal emission hot-spot effect on crop canopies. Two models, *Cupid* and *TRGM*, will be successively applied to simulate the thermal hot-spot signatures under conditions which cannot be easily captured in reality. The investigation will include the planting row structure, LAI, LAD, the component temperature distribution, as well as variations in the microclimate.

Section II provides a brief description of the methodology. Section III shows the simulation results and presents the quantitative relations between hot-spot amplitude and component temperature differences. Section IV presents conclusion and discussions. This paper represents the first part of a series of three related studies. The second part will focus on the validation using both airborne data and ground measurements. The last part will mainly deal with application issues.

II. Methodology

A. Definitions

Based on the work by Bréon *et al.* [10], Camacho de Coca *et al.* propose a model to represent the hot-spot reflectance signatures [15]. The model accounts for a multiple scattering effect and predicts canopy reflectance measurements using a four-parameter function

$$R = \frac{\Delta R_{\mathrm{HS}}}{1 + \xi/\xi_0} + b\xi + c \tag{1}$$

where R is the predicted reflectance, ξ is the phase angle, ΔR_{HS} is the hot-spot amplitude, ξ_0 is the hot-spot half width, and b and c are two empirical parameters. The half width is related to the canopy architecture, including LAI, canopy height, and leaf diameter. The fitted model reproduces very accurately the hot-spot directional signature [15]. It has been shown to be consistent with the research results from model calculations by Qin and Goel [11], laboratory measurements by Sandmeier *et al.* [16], and airborne data [17]. They all found that the hot-spot width may be quantified as the angular range in which normalized reflectance is greater than 0.5.

As mentioned above, there is no unique and commonly accepted method to derive the hot-spot width and amplitude in TIR for any component temperature distribution, especially when the soil temperature is lower than the leaf temperature. The sunlit part of the soil or leaf is normally warmer than the shadowed part, which makes the hot-spot signal of brightness temperature somehow similar with that of VNIR. Therefore, we propose to use a model similar to (1) to assess the hot-spot width and amplitude as

$$T_B(\theta) = \frac{\Delta T_{\mathrm{HS}}}{1 + \frac{|\theta - \theta_s|}{\xi_0}} + b(\theta - \theta_s) + c \tag{2}$$

where $T_B(\theta)$ is the directional brightness temperature at the view zenith of θ, ΔT_{HS} is the thermal emission hot-spot amplitude, and θ_s is the zenith angle of the sun. After fitting the model using a limited range of angles around θ_s, the ΔT_{HS} and ξ_0 are determined.

To conveniently compare different directional curves, $T_B(\theta)$ is rescaled to be $\Delta T_B(\theta)$ by subtracting $T_B(\theta_s)$ as follows:

$$\Delta T_B(\theta) = T_B(\theta) - T_B(\theta_s). \tag{3}$$

B. Simulation Models: TRGM and Cupid

To calculate the directional brightness temperature distribution, we use a thermal version of the computer-graphics-based model *TRGM* [18]. This model takes into account the 3-D architecture of the canopy and fully incorporates multiple scattering, shading, and mutual shadowing effects (including the hot-spot effect) and calculates the thermal radiation regime in the canopy. Its outputs include canopy $T_B(\theta)$, which is used in this study.

An energy balance model, named *Cupid*, is used to provide reasonable component temperature information for *TRGM*. The *Cupid* model, which was originally developed by Norman [19], was adapted and expanded by Huang *et al.* [20].

The selection of *Cupid* and *TRGM* represents a balance between computation accuracy and model efficiency. The *Cupid* model accounts for LAD and its effect on leaf temperature distribution more accurately than other models such as SHAW [21] and ISBA [22]. Processing time is faster than 3-D models such as DART EB [23]. The extended *Cupid* [20] further separates the sunlit and shadowed soil, which satisfies the basic requirement of component temperature distribution for realistic hot-spot simulation. Based on 3-D realistic scene and component temperature distribution, *TRGM* [18] can solve the radiance of each facet and is able to output the final directional effect with high accuracy for any inhomogeneous crop canopies. *TRGM* is more feasible and accurate than those row crop models (e.g., [7]). These two models were both originally developed for crop canopies and it is feasible to link them.

C. Test Sites

Two sites, including the winter wheat canopy in Beijing ($40°11'40''$N, $116°34'33''$E) and the summer corn canopies in Gansu ($38°51'25''$N, $100°24'38''$E), were chosen to acquire necessary input/output data and test the thermal emission hot-spot effect. The experiment in wheat canopies is related to the work of Liu *et al.* [24]. The experiment in the corn field is

TABLE I
CANOPY STRUCTURAL PARAMETERS

Plot	Acronym	Date	Canopy Height (m)	LAI	Leaf width (cm)	Leaf length (cm)	Row spacing (cm)
Wheat	W1	April 1 to April 21, 2001	0.1 - 0.4	0.5– 2.3	0.35-0.75	3-12	15
Corn	C1	June 11 to July 11, 2008	0.6 – 1.70	1.0-5.3	2.5 - 8	20-85	50

TABLE II
ENVIRONMENTAL PARAMETERS OF THE PLOTS AT LOCAL 10:30 am[a]

Plot	Date	T_a (℃)	P_w (mb)	U (m/s)	R_s (Wm^{-2})	W_{20} (%)	D_s (m)	T_{depth} (℃)
W1	April 1 to April 21,2001	10 - 25	3 - 20	0 - 4	200 - 700	5 – 30	1.0	20
C1	June 11 to July 11, 2008	18 – 26	9 – 16.7	0 – 4.3	100 - 800	30 – 33	1.6	16

[a] T_a, U, P_w, R_s, and W_{20} are the air temperature, wind speed, vapor pressure, downward solar radiation at 2-m height above ground, and volume water content of soil at 20 cm; D_s and $T_{\rm depth}$ are the lower boundary depth and soil temperature at that depth.

part of a large field campaign involving the project *WATER*: Watershed Allied Telemetry Experimental Research [25]. The input data include canopy structural parameters (see Table I), meteorological conditions, lower boundary conditions, and soil water content (see Table II). In the 4–14-μm range, the leaf emissivity varies from 0.978 to 0.994, and the soil emissivity ranges from 0.853 to 0.983. The *Cupid* model requires broadband emissivity as input, which is set at 0.95 and 0.97 for soil and leaf, to solve the component temperature distribution. The sky brightness temperature was calculated using the SKYIR function of the *Cupid* model which uses the air temperature and air humidity to estimate the air emissivity. The major output parameter is $T_B(\theta)$.

The soil types of the wheat and corn test sites are both silty loam. Based on the above datasets, the *Cupid* model calculates the component temperature distributions. The results at 10:30 am and 14:00 pm are extracted for analysis. The maximum soil temperatures $(T_{\rm soil})$ are 38 °C and 48 °C for wheat and corn respectively. The maximum difference between the sunlit and shadowed soil temperature is 8 °C for wheat canopies and 14 °C for corn canopies. The maximum difference between the leaf temperatures $(T_{\rm leaf})$ of the sunlit part and shadowed part is 4 °C for wheat canopies and 6 °C for corn canopies.

D. Generating Virtual Crop Canopies

Virtual wheat and corn canopies were generated by the MELS software [26] to represent different growth stages. In addition, a series of simple canopies were generated for sensitivity analysis (Fig. 1). In the simple canopies, the leaves are represented by isoceles triangles; the soil has no roughness. There are two reasons for choosing triangles to represent the leaves: 1) any arbitrary polygon can be seen as a group of triangles and 2) the shape of a triangle is easy to adjust. All of the scenes have a size of 1 m × 1 m and the height is 0.5 m. The basic leaf has a hemline length of 2.5 cm and a height of 2.5 cm. Three kinds of LAD (uniform distribution and erectophile and planophile distribution) were simulated. The control parameters include the row direction, row width, LAI, and leaf size. The row spacing is fixed at 50 cm. The azimuth angle in north is defined as zero for both the sun and row directions.

E. Simulations of the Thermal Emission Hot Spots

Realistic and random simulations were both performed by *TRGM* to produce $T_B(\theta)$ in SPP after *Cupid* simulations. In the realistic simulation, the component temperatures were assigned to polygons by height, orientation, and sunlit fraction for virtual wheat and corn canopies each half hour during the dates (see Table I). The sun position varied from day to night. The random simulation used the triangular scenes and selected a few subsets of *Cupid* simulations of component temperatures for sensitivity analysis. In the random simulation, the solar zenith and azimuth angles were fixed at 30° and 120°, respectively. We used the center wavelengths of the bands of MODIS, the Moderate Resolution Imaging Spectroradiometer, to simulate the directional effects in 16 bands from 4 to 14 μm. Based on (2), the curve fitting function in MATLAB 6.5 (MathWorks Inc.) automatically calculates the hot-spot amplitude and half width. Finally, a look-up table (LUT) presented in Table III is created for sensitivity analysis. This table includes the input parameters (e.g., component temperature, LAI, LAD, leaf size/canopy height, and row direction) and the output parameters (hot-spot amplitude/half width).

F. Inverting Component Temperature Differences

The temperature differences between the shadowed and sunlit parts of soil/leaf contain rich information about heat-water status for soil [27]. Brightness of shadows is determined by diffuse radiation only, causing temperature difference between the shadow and its adjacent sunlit surface. Since the major factor affecting thermal emission hot-spot effect is the component temperature difference, there is a potential to use hot-spot information to retrieve the component temperature differences.

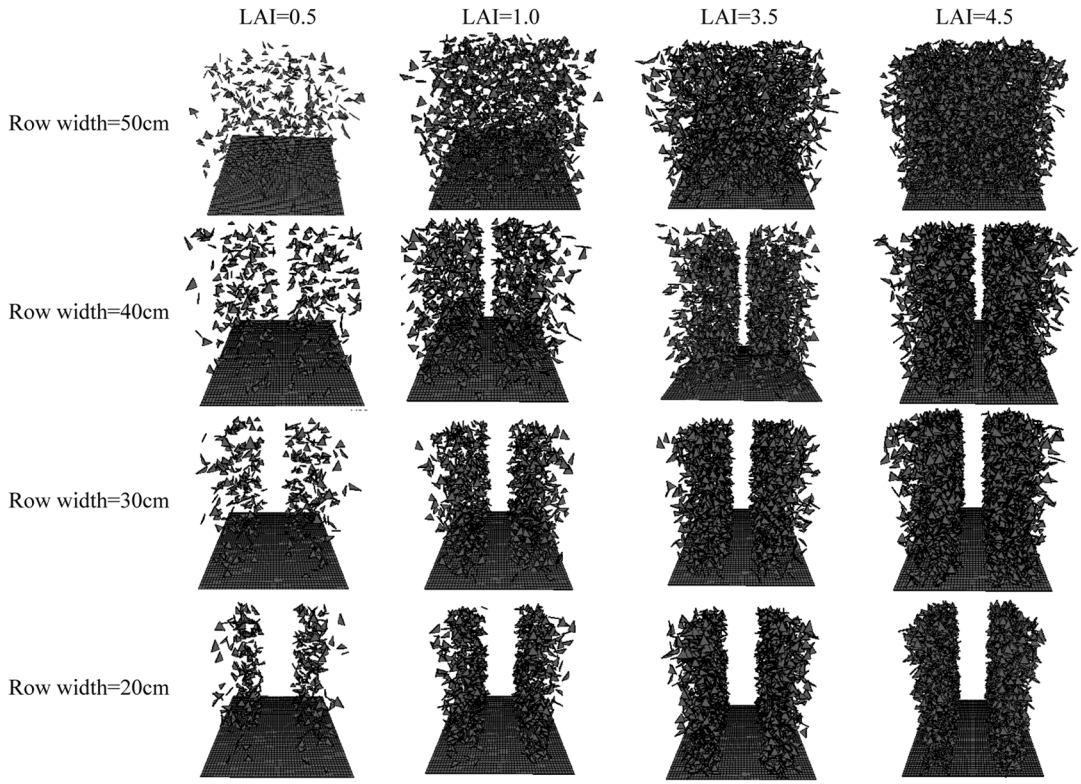

Fig. 1. Three-dimensional row-structural canopies for sensitivity analysis with a uniform LAD, LAI's ranging from 0.5 to 4.5, and row widths from 20 to 50 cm.

TABLE III
SAMPLE OF LUT FOR SENSITIVITY ANALYSIS[a]

ΔT_{HS} (℃)	ξ_0 (°)	$T_{s,lit}$ (℃)	$T_{s,shd}$ (℃)	$T_{l,lit}$ (℃)	$T_{l,shd}$ (℃)	LAI	H (cm)	S_l (cm)	φ (°)	G	L_w (cm)
0.5	1.5	40	38	20	20	0.5	50	2.5	90	0.5	20
1.0	1.6	40	36	20	18	1.0	100	2.5	90	0.5	30
2.0	5.0	40	39	25	20	5.0	100	3.0	50	0.2	40
…				…							…
10	3.4	46	31	21	18	1.5	200	5.0	0	0.8	50

[a] $T_{s,\mathrm{lit}}$, and $T_{s,\mathrm{shd}}$ are sunlit and shadowed soil temperature; $T_{l,\mathrm{lit}}$, and $T_{l,\mathrm{shd}}$ are the sunlit and shadowed leaf temperature; S_l is the leaf size represented by the height of isoceles triangle; H is the canopy height; φ is the azimuth difference between sun and row direction; G is the G-function; L_w is the row width.

According to the Geometric Optical (GO) model, the observed radiance can be estimated as the sum of component radiances

$$B_\lambda\left(T_B(\theta)\right) = \sum_{i=1}^{4} f_i(\theta) \times B_\lambda(T_i) \tag{4}$$

where B is the Planck function, λ represents wavelength, T_i ($i = 1, 2, 3, 4$) is the brightness temperatures for the sunlit soil, the shadowed soil, the sunlit leaf, and the shadowed leaf, respectively, and $f_i(\theta)$ represents the corresponding component view fractions at the direction θ. According to the definition of the hot-spot half width (ξ_0) and (2), the hot-spot amplitude can be estimated as the difference between $T_B(\theta_s)$ and $T_B(\theta_s \pm \xi_0)$ as

$$\Delta T_{HS} = \left[T_B(\theta_s) - T_B(\theta_s - \xi_0)\right] + \left[T_B(\theta_s) - T_B(\theta_s + \xi_0)\right]. \tag{5a}$$

In the TIR range, the monochromatic radiance can be linearly related to the brightness temperature by a first-order Taylor series expansion of the Planck function [28]–[30]. Prata demonstrated the high-accuracy performance of the linearization (better than 1%) for a moderate departure (<10 K) from the expansion point from 10 to 13 μm within the temperature range 270 K–320 K [29]. Since the difference between $T_B(\theta_s)$ and $T_B(\theta_s \pm \xi_0)$ is generally less than 10 K, (5a) can be rewritten as

$$\begin{aligned}\Delta T_{\mathrm{HS}} &= \frac{B_\lambda\left(T_B(\theta_s)\right) - B_\lambda\left(T_B(\theta_s + \xi_0)\right)}{\partial B_\lambda\left(T_B(\theta_s)\right)/\partial T} \\ &\quad + \frac{B_\lambda\left(T_B(\theta_s)\right) - B_\lambda\left(T_B(\theta_s - \xi_0)\right)}{\partial B_\lambda\left(T_B(\theta_s)\right)/\partial T} \\ &= \frac{\sum_{i=1}^{4} B_\lambda(T_i) \times \left[2 f_i(\theta_s) - f_i(\theta_s - \xi_0) - f_i(\theta_s + \xi_0)\right]}{\partial B_\lambda\left(T_B(\theta_s)\right)/\partial T}.\end{aligned} \tag{5b}$$

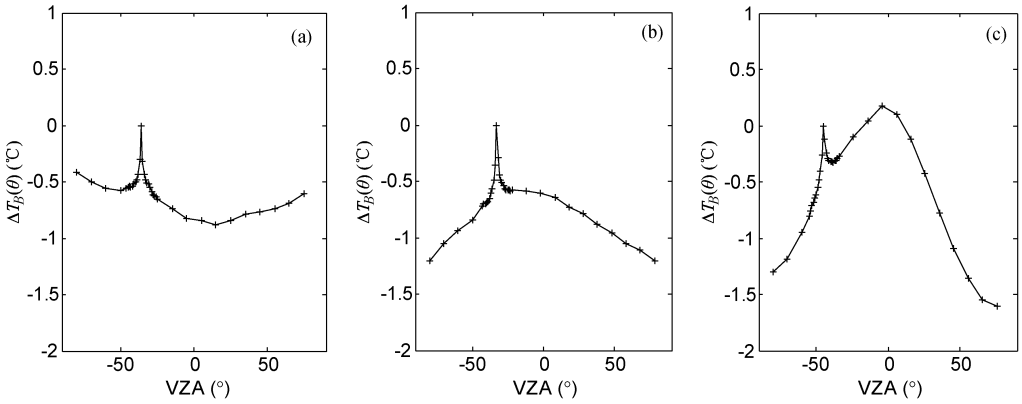

Fig. 2. Three typical directional signatures found in the simulation study: (a) bowl-shaped, (b) dome-shaped, and (c) bell-shaped.

When the view direction coincides with the solar direction, fractions f_2 and f_4 for the shadowed soil and leaf are zero. When θ equals $\theta_s \pm \xi_0$, the shadow fractions f_2 and/or f_4 are increasing and the sunlit fractions f_1 and/or f_3 are decreasing since the sum of the four fractions equals 1.0. Since ξ_0 is usually small, e.g., less than 3° by Camacho de Coca *et al.* [15], the total view fractions of the soil or leaf can be assumed to be linearly varying within the range $[\theta_s - \xi_0, \theta_s + \xi_0]$. Therefore, there exist quantitative relationships between the fractions as follows:

$$\begin{aligned} 2f_1(\theta_s) &= [f_1(\theta_s - \xi_0) + f_2(\theta_s - \xi_0)] \\ &\quad + [f_1(\theta_s + \xi_0) + f_2(\theta_s + \xi_0)] \\ 2f_3(\theta_s) &= [f_3(\theta_s - \xi_0) + f_4(\theta_s - \xi_0)] \\ &\quad + [f_3(\theta_s + \xi_0) + f_4(\theta_s + \xi_0)] \end{aligned} \tag{6}$$

and the hot-spot amplitude can be rewritten as

$$\begin{aligned} \Delta T_{\mathrm{HS}} = &[f_2(\theta_s - \xi_0) + f_2(\theta_s + \xi_0)] \frac{B_\lambda(T_1) - B_\lambda(T_2)}{\partial B_\lambda\left(T_B(\theta_s)\right)/\partial T} \\ &+ [f_4(\theta_s - \xi_0) + f_4(\theta_s + \xi_0)] \frac{B_\lambda(T_3) - B_\lambda(T_4)}{\partial B_\lambda\left(T_B(\theta_s)\right)/\partial T}. \end{aligned} \tag{7a}$$

By assuming that the brightness temperature differences $(T_1 - T_2)$ and $(T_3 - T_4)$ are relatively small, (7a) becomes

$$\begin{aligned} \Delta T_{HS} = &[f_2(\theta_s - \xi_0) + f_2(\theta_s + \xi_0)] \\ &\times \frac{\partial B_\lambda(T_2)/\partial T}{\partial B_\lambda\left(T_B(\theta_s)\right)/\partial T}(T_1 - T_2) \\ &+ [f_4(\theta_s - \xi_0) + f_4(\theta_s + \xi_0)] \\ &\times \frac{\partial B_\lambda(T_3)/\partial T}{\partial B_\lambda\left(T_B(\theta_s)\right)/\partial T}(T_3 - T_4). \end{aligned} \tag{7b}$$

When the differences between $T_B(\theta_s)$ and T_2 or $T_B(\theta_s)$ and T_3 are small (less than 10 K), the two ratios of differential coefficients are assumed to be 1. Then, assuming that the sunlit and the shadowed parts receive the same diffuse irradiance from surrounding leaf/soil elements, the brightness temperature differences $(T_1 - T_2)$ and $(T_3 - T_4)$ can be linearly transferred to the thermodynamic component temperature differences by multiplying the soil emissivity $(\varepsilon_{\mathrm{soil}})$ and the leaf emissivity $(\varepsilon_{\mathrm{leaf}})$, respectively. Finally, the hot-spot amplitude can be derived as follows:

$$\begin{aligned} \Delta T_{\mathrm{HS}} = &[f_2(\theta_s - \xi_0) + f_2(\theta_s + \xi_0)]\, \varepsilon_{\mathrm{soil}} \Delta T_{\mathrm{soil}} \\ &+ [f_4(\theta_s - \xi_0) + f_4(\theta_s + \xi_0)]\, \varepsilon_{\mathrm{leaf}} \Delta T_{\mathrm{leaf}}. \end{aligned} \tag{8}$$

Equation (8) presents the theoretical expression of a linear relationship between the hot-spot amplitude and the component temperature differences (ΔT_{soil} and ΔT_{leaf}) under normal conditions. It can be seen that both differences contribute to ΔT_{HS}. The contributions affected by the four view fractions are complex and difficult for practical use. However, when LAI is large, f_2 can be omitted and ΔT_{leaf} can be solved from ΔT_{HS}. Similarly, ΔT_{soil} can be calculated when f_4 can be neglected. Therefore, a statistical approach was adopted to simplify (8) and derive ΔT_{leaf} and ΔT_{leaf} separately from ΔT_{HS}. Because the view fractions usually have an exponential form, Gaussian function was found to produce a good fit for ΔT_{leaf} and ΔT_{soil}.

III. Simulation Results

A. Thermal Emission Hot-Spot Signatures and Curve Fitting

The analysis of the $T_B(\theta)$ results of the virtual wheat canopies for a 20-day period revealed three typical kinds of directional signatures, which are bowl-shaped, dome-shaped, and bell-shaped (Fig. 2).

The bowl and dome shapes resemble the BRF in VNIR. In contrast, the bell shape is special for TIR because the hot spot $T_B(\theta_s)$ is weak and lower than $T_B(0)$. Each type normally corresponds to a different canopy structure and component temperature distribution (the subscript "lit" and "shd" representing the sunlit and shadowed part, respectively):

- Bowl shape—T_{leaf} is greater than T_{soil}, and $T_{soil,lit}$ is greater than $T_{soil,shd}$.
- Dome shape—T_{soil} is greater than T_{leaf}, and $T_{\mathrm{soil,lit}}$ is significantly greater than $T_{\mathrm{soil,shd}}$.
- Bell shape—T_{soil} is greater than T_{leaf}, and $T_{\mathrm{soil,lit}}$ is slightly greater than $T_{\mathrm{soil,shd}}$.

However, it is not necessary to fit (2) separately to each one of the three kinds of shapes. The $T_B(\theta)$ near the solar zenith angle (e.g., $\pm 10°$) can be estimated for all three using (2). Using

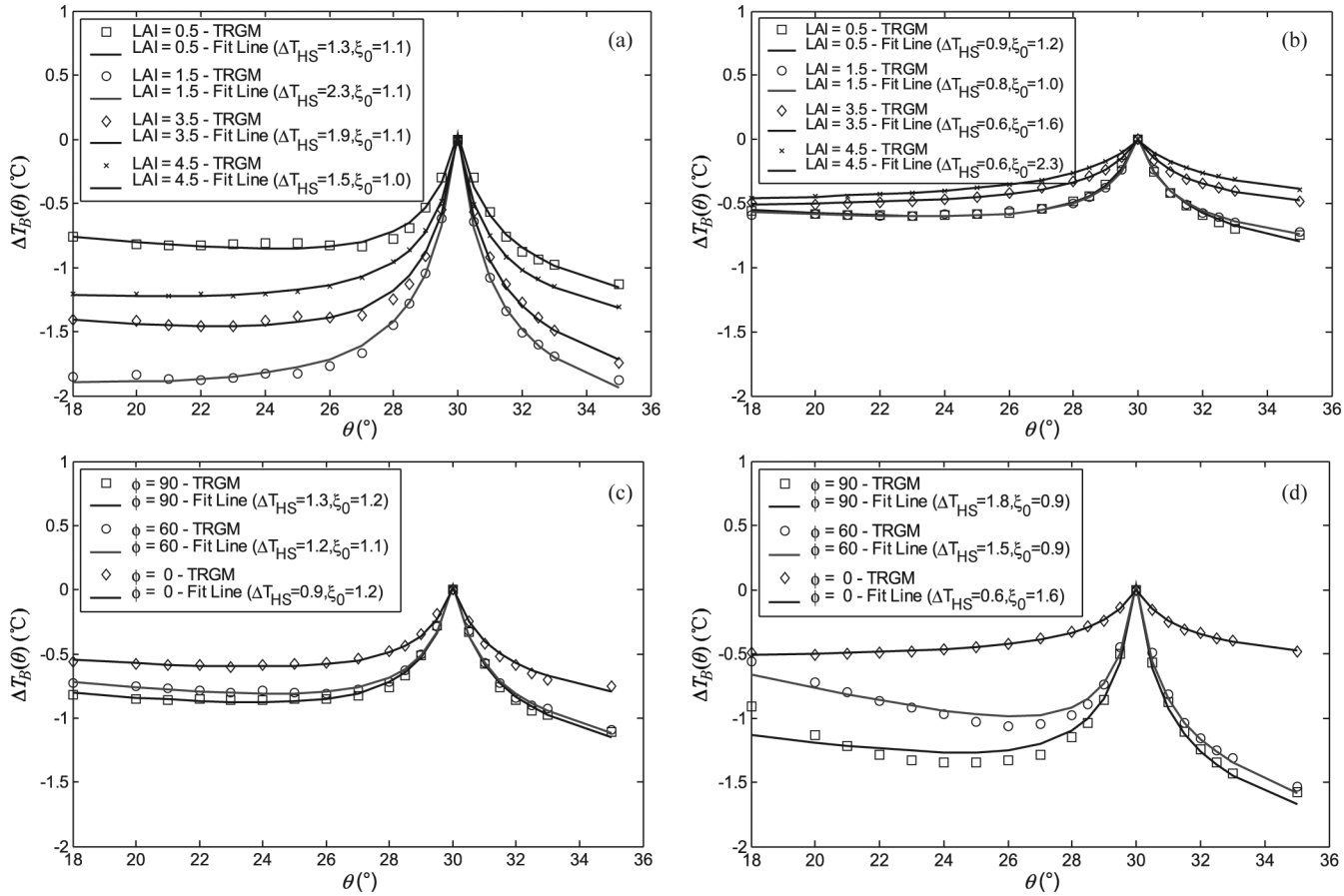

Fig. 3. Directional signatures of hot spot derived from the sensitivity analysis. (a) LAI effect (row width $= 50$ cm). (b) LAI effect (row width $= 20$ cm). (c) View azimuth effect (LAI $= 4.5$, row width $= 50$ cm). (d) View azimuth effect (LAI $= 0.5$, row width $= 20$ cm). The points represent the simulation results of *TRGM*. The lines indicate the results of the best fit for the model defined in (2). The retrieved values of hot-spot amplitude and half width are shown on the legend. The component temperatures are fixed ($T_{s,\mathrm{lit}} = 46\,^{\circ}\mathrm{C}$, $T_{s,\mathrm{shd}} = 39\,^{\circ}\mathrm{C}$, $T_{l,\mathrm{lit}} = 35\,^{\circ}\mathrm{C}$, $T_{l,\mathrm{shd}} = 32\,^{\circ}\mathrm{C}$).

$T_B(\theta)$ between $\theta_s - 10$ and $\theta_s + 10$, the R^2 of fitting was found to be always greater than 0.98 while the RMSE was around 0.04 °C. Fig. 3 shows a selection of curve-fitting results which demonstrate the hot-spot signatures and their variation with the main control parameters. It can be seen that the planting row structure can significantly affect the ΔT_{HS} and reduce its value by a maximum amount of about 1.2 °C when compared with an unstructured horizontal canopy. However, this result is limited by a set of simulation which may not cover all cases. More simulations under a wider range of conditions will be done in the future.

B. Comparing Reflectance Hot Spot and Thermal Emission Hot Spot

To compare with the hot spot in VNIR, the bidirectional reflectance factor (BRF) in the RED (660 nm, leaf reflectance and transmittance $= 0.05$) and the NIR (780 nm, leaf reflectance and transmittance $= 0.48$) are also simulated with *TRGM*. Fig. 4 shows the scatter plots of the half width and the amplitude among the three bands. The ΔR_{HS} is the reflectance hot-spot amplitude obtained by fitting the relative reflectance ($\Delta R(\theta) = \mathrm{BRF}$ minus the hot spot reflectance) to (1). Both the half width and amplitude of the RED band are highly correlated with those of TIR [Fig. 4(a) and (b)]. However, the correlation between the NIR and TIR band is poor [Fig. 4(c) and (d)].

Additional simulations have shown that the thermal ξ_0 normally increases with leaf size. This trend resembles those of the RED band more than that in NIR. If the soil emissivity is kept constant, the ξ_0 and ΔT_{HS} from 4 to 14 μm is nearly not affected by wavelength. Even when the soil emissivity changes from 0.89 to 0.95, ΔT_{HS} variation is within 0.2 °C. Since ΔT_{HS} varies little with wavelength, the 14-μm was selected for the following analysis, where the soil and leaf emissivities are 0.02 and 0.01, respectively.

C. Relationship Between Emission Hot-Spot Amplitude and Component Temperature Differences

Based on the *LUT* in Table III, good correlations ($R^2 = 0.88$, $\mathrm{RMSE} = 0.5\,^{\circ}\mathrm{C}$) are found between the hot-spot amplitude and the differences of sunlit and shadowed temperature of soil and leaf at 14 μm as follows:

$$\Delta T_{\mathrm{HS}} = 0.28 \times \mathrm{e}^{-\left(\frac{G\times\Omega\times\mathrm{LAI}}{2.5}\right)^2}\Delta T_{\mathrm{soil}} + 0.35 \times \mathrm{e}^{-\left(\frac{G\times\Omega\times\mathrm{LAI}-5.0}{5.0}\right)^2}\Delta T_{\mathrm{leaf}} \quad (9)$$

where Ω is the ratio of row width to row spacing which represents the row width effect, and G is the well-known G-function (0.5 for spherical canopy) proposed by Ross and Nilson [31].

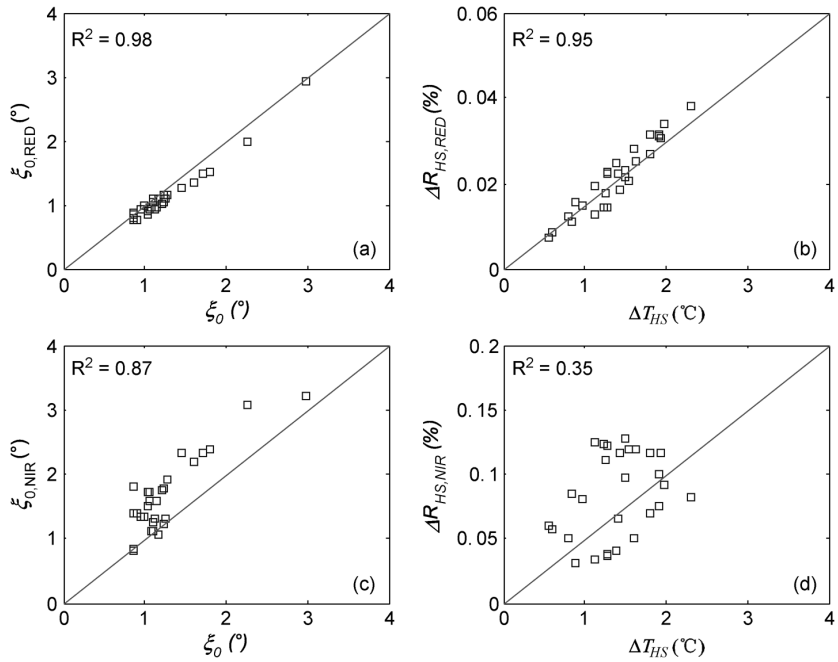

Fig. 4. Comparisons of hot-spot half width and amplitude among the RED, the NIR, and the TIR band. (a) Scatter plots of ξ_0 between RED and TIR. (b) Scatter plots of hot-spot amplitude between RED and TIR. (c) Scatter plots of ξ_0 between NIR and TIR. (d) Scatter plots of the hot-spot amplitude between NIR and TIR. The lines in (a) and (c) are 1:1 lines. The diagonal lines in (b) and (d) are only used to improve interpretation. LAI ranges from 0.5 to 4.5; leaf size is 2.5 cm; the component temperatures are fixed ($T_{s,\mathrm{lit}} = 46\,^{\circ}\mathrm{C}$, $T_{s,\mathrm{shd}} = 39\,^{\circ}\mathrm{C}$, $T_{l,\mathrm{lit}} = 35\,^{\circ}\mathrm{C}$, $T_{l,\mathrm{shd}} = 32\,^{\circ}\mathrm{C}$).

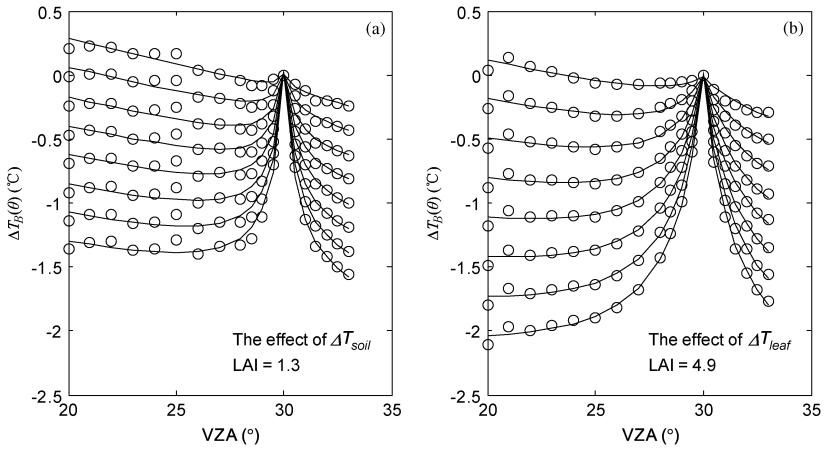

Fig. 5. Effect of component temperature differences on hot-spot effect over horizontal canopies. (a) Effect of ΔT_{soil} when $T_{s,\mathrm{shd}} = 32$–$40\,^{\circ}\mathrm{C}$ by fixing the other three temperatures ($T_{s,\mathrm{lit}} = 40\,^{\circ}\mathrm{C}$, $T_{l,\mathrm{lit}} = 20\,^{\circ}\mathrm{C}$, $T_{l,\mathrm{shd}} = 25\,^{\circ}\mathrm{C}$). (b) Effect of ΔT_{leaf} when $T_{l,\mathrm{shd}} = 25$–$33\,^{\circ}\mathrm{C}$ by fixing the other three temperatures ($T_{s,\mathrm{lit}} = 40\,^{\circ}\mathrm{C}$, $T_{s,\mathrm{shd}} = 40\,^{\circ}\mathrm{C}$, $T_{l,lit} = 25\,^{\circ}\mathrm{C}$). The lines are fitted by using (2). From top to bottom, the lines represent the temperature differences increasing from 0 to 8 °C in steps of 1 °C.

Consistent with the theoretical deduction of (8), the good fitting result partly proved its rationality. Since (9) is an indefinite equation, it is difficult to inverse ΔT_{leaf} and ΔT_{soil} simultaneously without additional information. However, a piecewise approximation method could be used according to the simulation results that the leaf temperature difference $(\Delta T_{\mathrm{leaf}})$ significantly contributes to the hot-spot amplitude when LAI is greater than 4.0, while the soil temperature difference $(\Delta T_{\mathrm{soil}})$ affects the hot-spot amplitude when LAI is less than 5.0. Fig. 5(a) shows that ΔT_{HS} increases from 0 to nearly 1.5 °C as ΔT_{soil} increases from 0 to 8 °C and LAI is set to 1.3. When ΔT_{leaf} increases from 0 to 8 °C and LAI is set to 4.9, ΔT_{HS} increases from 0 to nearly 2 °C [Fig. 5(b)]. When the planting row width decreases, the same trend occurs except smaller amplitude. Finally, the piecewise predication equation for the two temperature differences is presented as follows:

$$\begin{aligned} \Delta T_{\mathrm{soil}} &= a \times \mathrm{e}^{\left(\frac{G\times\Omega\times\mathrm{LAI}}{2.5}\right)^2} \Delta T_{\mathrm{HS}}, \qquad \mathrm{LAI} < 5.0 \\ \Delta T_{\mathrm{leaf}} &= q \times \mathrm{e}^{\left(\frac{G\times\Omega\times\mathrm{LAI}-5.0}{5.0}\right)^2} \Delta T_{\mathrm{HS}}, \qquad \mathrm{LAI} \geq 4.0 \end{aligned} \quad (10)$$

where a and q are two empirical parameters with default values at 3.57 and 2.86, respectively, which is slightly affected by soil or leaf emissivity. The two thresholds of LAI are not so strict and can slightly vary with different row structures, depending on LAD and the orientation and width of the rows.

The component temperatures and ΔT_{HS} in the *LUT* were used to assess the performance of (10). Results show that the accuracy is high in horizontal canopies (row width $= 50$ cm) for ΔT_{leaf} ($\mathrm{RMSE} = 0.2\,^{\circ}\mathrm{C}$, $R^2 = 0.99$) and ΔT_{soil} ($\mathrm{RMSE} = 0.4\,^{\circ}\mathrm{C}$, $R^2 = 0.99$). The estimation error of ΔT_{leaf} and ΔT_{soil} will increase if the planted row width decreases and row structure becomes significant. Nevertheless, the accuracy is still acceptable ($\mathrm{RMSE} < 1.8\,^{\circ}\mathrm{C}$, $R^2 > 0.81$) when the row width is greater than 25 cm. To further evaluate (10), we randomly generated 1000 new groups of input parameters with the same structure as Table III and used *TRGM* to simulate the directional effects. The ΔT_{HS} were then extracted using (2). Based on this set of data, the accuracy of (10) was assessed and found to be still within the range ($\mathrm{RMSE} < 1.8\,^{\circ}\mathrm{C}$, $R^2 > 0.81$). Additional validation will be presented in the subsequent part of this series.

These results derived from (9) and (10) are based on the assumption that the virtual leaves are triangular. To evaluate the performance in virtual wheat and corn canopies, we use (10) to invert the component temperature differences and compare the results with the input component temperatures at two points in time (10:30 am and 14:00 pm) in all the simulated days. The RMSE and R^2 for the inversion of ΔT_{soil} in the wheat canopies are 0.75 °C and 0.81, respectively. The inversion accuracies of ΔT_{leaf} in the corn canopies are also high ($\mathrm{RMSE} = 1.0\,^{\circ}\mathrm{C}$, $R^2 = 0.89$) when LAI is greater than 4.0. However, the inversion accuracies of ΔT_{soil} in the corn canopies are slightly lower ($\mathrm{RMSE} = 1.8\,^{\circ}\mathrm{C}$, $R^2 = 0.85$). If incorporated with prior knowledge of component temperature distribution, (9) would be invertible and the inversion accuracies should be improved. Nevertheless, these results suggest that (9) and (10) be useful for studies with virtual crop canopies.

IV. Conclusion and Discussions

A. Conclusion

The thermal emission hot-spot effect of crop canopies was investigated in detail by model simulation. The simulation results obtained in this study show that there are typically three types of directional thermal emission shape in SPP, namely, *bowl*, *dome*, and *bell* shapes. Regardless of the shape, a curve-fitting model was proposed to derive the hot-spot amplitude and half width with three independent variables: the phase angle ξ, the hot-spot amplitude ΔT_{HS}, and the half width ξ_0. The accuracy of the fitting model is good ($R^2 = 0.98$ and $\mathrm{RMSE} = 0.04\,^{\circ}\mathrm{C}$). Based on the curve-fitting model, a new algorithm that predicts the component temperature differences from hot-spot amplitude was presented, whose accuracy was found to be good for the horizontal canopies with triangular leaves ($\mathrm{RMSE} < 0.4\,^{\circ}\mathrm{C}$ and $R^2 = 0.99$), and acceptable for the virtual wheat and corn canopies with planting row structure ($\mathrm{RMSE} < 1.8\,^{\circ}\mathrm{C}$ and $R^2 > 0.81$).

To our knowledge, the subject presented here is new and can be used for inverting component temperature differences, which provide helpful information for estimating soil water content or evapotranspiration in land surface energy balance research. In the subsequent papers of this series, we will validate our prediction algorithm and deal with application issues.

B. Discussions

There are still two limitations of our simulation work. The first one is the single solar direction used in one view plane (SPP) for sensitivity analysis and equation derivation. The higher errors of virtual wheat and corn canopies than those of simple canopies are mainly due to the different sun positions with θ_s varying from 20° to 48°. The other limitation is not considering the discrete structure of clusters in each row for sparse canopies, which produced the largest error of ΔT_{soil} for corn canopies. More simulations under a wider range of conditions, including cases on other solar directions and viewing planes and discrete row structures, will be done in the future.

Despite the limitations, (9) and (10) will have the potential to help derive soil water content from remote sensing data. Zhang *et al.*, based on ground measurement which is solid and useful at ground scales, found that ΔT_{soil} and ΔT_{leaf} are a function of soil water content and developed an inversion model based on normal wind speed and solar radiation data from a weather station [27]. The input remote sensing data are the four component temperatures. The accuracy of their model explains about 85% of the variation. However, at airborne or satellite scales, more complicated inversion processes are required to derive the four component temperatures. Our study proposes an alternative possibility to invert component temperature differences from hot-spot amplitude. Using our component temperature differences instead as input, we are able to utilize the soil water inversion algorithm by Zhang *et al.* [27] to predict soil water content at a larger scale. Relevant details will be presented in a subsequent study.

The simulation analysis has also demonstrated an interesting new discovery relating to the similarity of hot spot between the RED band and the TIR band. We attribute this similarity to the same low level of reflectance of leaf and soil in TIR and RED band. Li *et al.* conclude that the thermal emission directionality is determined by both the BRDF-derived emissivity and the distribution patterns of temperature differences [32], [33]. Therefore, when the temperature distribution is fixed, the thermal emission directionality is mainly controlled by component reflectances/emissitivies. The main reason why the NIR and TIR hot spots are poorly related is due to more multiple scattering in the NIR, which reduces the hot-spot effect. This finding can help us to derive the thermal hot-spot half width from the RED band, which is easier to measure by currently operating sensors, such as POLDER (POLarization and Directionality of Earth Reflectances). However, the half width of the thermal emission hot spot also contains rich information of the canopy geometry architecture, such as leaf size, LAD, row width, and so on. If combined with the half width in VNIR, the estimation accuracy of canopy architecture could be improved.

Moving forward to practical implementation from the laboratory investigation/experiment, more work is needed. The first issue to address is the reliable measurement of the thermal emission hot-spot effect. Yu *et al.* used a thermal camera equipped with a wide angle lens and successfully captured the emission hot-spot effect [7]. Their work confirmed the possibility to use a wide angle lens to obtain the hot-spot features from ground-based measurements. In the second part of our

article, we will use a similar method to validate our simulation results. The second issue is the limited amount of directional observations of current real satellite data. Fortunately, Vermote and Roy demonstrated the evidence of hot-spot observation in successive MODIS scans due to a wide scan angle without using multiple images with different view angles [34]. Therefore, it is also possible to observe the thermal emission hot-spot effect from MODIS. Furthermore, we expect future TIR sensors to have the capability of directly observing hot-spot effect.

ACKNOWLEDGMENT

The authors would like to thank K. v. Gadow and the kind reviewers for their helpful comments.

REFERENCES

[1] W. Qin and Y. Xiang, "On the hotspot effect of the leaf canopies: Modeling study and influence of leaf shape," *Remote Sens. Environ.*, vol. 50, pp. 95–106, 1994.

[2] L. K. Balick and B. A. Hutchinson, "Directional thermal infrared exitance distributions from a leafless deciduous forest," *IEEE Trans. Geosci. Remote Sens.*, vol. GE-24, no. 5, pp. 453–458, Sep. 1986.

[3] D. L. B. Jupp, "Directional radiance and emissivity measurement models for remote sensing of the surface energy balance," *Environ.Modelling Software*, vol. 13, no. 3, pp. 341–351, Oct. 1998.

[4] J. P. Lagouarde, Y. H. Kerr, and Y. Brunet, "An experimental study of angular effects on surface temperature for various plant canopies and bare soils," *Agricult. Forest Meteorol.*, vol. 77, no. 3–4, pp. 167–190, Dec. 1995.

[5] J.-P. Lagouarde, H. Ballans, P. Moreau, D. Guyon, and D. Coraboeuf, "Experimental study of brightness surface temperature angular variations of Maritime Pine (Pinus pinaster) stands," *Remote Sens. Environ.*, vol. 72, no. 1, pp. 17–34, Apr. 2000.

[6] Q. H. Liu, X. F. Gu, X. W. Li, F. Jacob, J. F. Hanocq, M. Friedl, A. H. Strahler, T. Yu, and G. L. Tian, "Study on thermal infrared emission directionality over crop canopies with TIR camera imagery," *Science in China (Series E)*, vol. 43, no. Supp, pp. 95–103, Dec. 2000.

[7] T. Yu, X. Gu, G. Tian, M. Legrand, F. Baret, J.-F. Hanocq, R. Bosseno, and Y. Zhang, "Modeling directional brightness temperature over a maize canopy in row structure," *IEEE Trans. Geosci. Remote Sens.*, vol. 42, no. 10, pp. 2290–2304, Oct. 2004.

[8] B. Hapke, "Theory of reflectance and emittance spectroscopy," in *Topics in Remote Sensing*. Cambridge, MA: Cambridge Univ. Press, 1993, vol. 3, p. 455.

[9] B. Hapke, D. Dimucci, R. Nelson, and W. Smythe, "The cause of the hot spot in vegetation canopies and soils: Shadow-hiding versus coherent backscatter," *Remote Sens. Environ.*, vol. 58, no. 1, pp. 63–68, Oct. 1996.

[10] F.-M. Bréon, F. Maignan, M. Leroy, and I. Grant, "Analysis of the hot spot directional signatures measured from space," *J. Geophys. Res.*, vol. 107, no. D16, pp. 4282–4296, Aug. 2002.

[11] W. Qin and N. S. Goel, "An evaluation of hotspot models for vegetation canopies," *Remote Sens. Rev.*, vol. 13, pp. 121–159, 1995.

[12] W. Qin, N. S. Goel, and B. Wang, "The hotspot effect in heterogeneous vegetation canopies and performance of various hotspot models," *Remote Sens. Rev.*, vol. 14, pp. 283–332, 1996.

[13] J. A. Smith and J. R. Ballard, "Thermal infrared hot spot and dependence on canopy geometry," *Opt. Eng.*, vol. 40, pp. 1435–1437, 2001.

[14] L. F. Chen, Q. H. Liu, W. J. Fan, X. Li, Q. Xiao, G. J. Yan, and G. L. Tian, "A bi-directional gap model of directional thermal radiation of row crops," *Science in China (Series D)*, vol. 45, no. 12, pp. 1087–1098, 2002.

[15] F. C. Coca, F.-M. Bréon, M. Leroy, and F. J. Garcia-Haro, "Airborne measurement of hot spot reflectance signatures," *Remote Sens. Environ.*, vol. 90, no. 1, pp. 63–75, Mar. 2004.

[16] S. Sandmeier, C. Muller, B. Hosgood, and G. Andreoli, "Sensitivity analysis and quality assessment of laboratory BRDF data," *Remote Sens. Environ.*, vol. 64, pp. 176–191, 1998.

[17] J. L. Privette and E. F. Vermote, "Fitting remote sensing data with linear bidirectional reflectance models," presented at the SPIE Symp. Satellite Remote Sens., Paris, France, Sep. 1995.

[18] Q. H. Liu, H. G. Huang, W. Qin, K. Fu, and X. Li, "An extended 3-D radiosity-graphics combined model for studying thermal-emission directionality of crop canopy," *IEEE Trans. Geosci. Remote Sens.*, vol. 45, no. 9, pp. 2900–2918, Sep. 2007.

[19] J. M. Norman, "Modeling the complete crop canopy," in *Modification of the Aerial Environment of Plants*, B. Barfield and J. Gerber, Eds. St. Joseph, MI: Amer. Soc. Agric. Eng., 1979, vol. 2, pp. 249–277.

[20] H. G. Huang, X. Xin, Q. H. Liu, Q. Liu, L. F. Chen, and X. Li, "Modeling soil component temperature distribution by extending CUPID model," in *Proc. IGARSS2006*, Denver, CO, 2006, pp. 1370–1373.

[21] G. N. Flerchinger and K. E. Saxton, "Simultaneous heat and water model of a freezing snow-residue-soil system I. Theory and development," *Trans. Amer. Soc. Agricult. Eng.*, vol. 32, no. 2, pp. 565–571, Mar.–Apr. 1989.

[22] J. Noilhan and J. F. Mahfouf, "The ISBA land surface parameterisation scheme," *Global and Planetary Change*, vol. 13, no. 1, pp. 145–159, Jun. 1996.

[23] J. P. Gastellu-Etchegorry, "3D modeling of satellite spectral images, radiation budget and energy budget of urban landscapes," *Meteorol. Atmosphe.c Phys.*, vol. 102, no. 3–4, pp. 187–207(21), Dec. 2008.

[24] Q. H. Liu, X. W. Li, and L. F. Chen, "Field campaign for quantitative remote sensing in Beijing," in *Proc. IGARSS'2002*, Toronto, ON, Canada, 2002, pp. 3133–3135.

[25] X. Li, X. W. Li, Z. Y. Li, M. G. Ma, J. Wang, Q. Xiao, Q. Liu, T. Che, E. X. Chen, G. J. Yan, Z. Y. Hu, L. X. Zhang, R. Z. Chu, P. X. Su, Q. H. Liu, S. M. Liu, J. D. Wang, Z. Niu, Y. Chen, R. Jin, W. Z. Wang, Y. H. Ran, X. Z. Xin, and H. Z. Ren, "Watershed allied telemetry experimental research," *J. Geophys. Res.-Atmospheres*, vol. 114, no. D22, p. D22103, Nov. 2009.

[26] W. Qin and S. A. W. Gerstl, "3-D scene modeling of semidesert vegetation cover and its radiation regime," *Remote Sens. Environ.*, vol. 74, no. 1, pp. 145–162, Oct. 2000.

[27] R. H. Zhang, H. B. Su, Z.-L. Li, X. M. Sun, X. Z. Tang, and F. Becker, "The potential information in the temperature difference between shadow and sunlit of surfaces and a new way of retrieving the soil moisture," *Science in China (Series D)*, vol. 44, no. 2, pp. 112–123, Feb. 2001.

[28] J. C. Price, "Land surface temperature measurements from the split window channels of the NOAA 7 advanced very high resolution radiometer," *J. Geophys. Res.*, vol. 89, no. D5, pp. 7231–7237, 1984.

[29] A. J. Prata, "Land surface temperatures derived from the AVHRR and ATSR, 1 theory," *J. Geophys. Res.*, vol. 89, no. D9, pp. 16689–16702, 1993.

[30] Z. Qin, G. Dall'Olmo, A. Karnieli, and P. Berliner, "Derivation of split window algorithm and its sensitivity analysis for retrieving land surface temperature from NOAA-advanced very high resolution radiometer data," *J. Geophys. Res.*, vol. 106, no. D19, pp. 22655–22670, Oct. 2001.

[31] J. K. Ross and T. A. Nilson, "A mathematical model of radiation regime of the plant cover," in *Actinometry and Atmospheric Optics* (in Russian). Tallinn, Russia: Valgus, 1968, pp. 263–281.

[32] X. Li, A. H. Strahler, and M. A. Friedl, "A conceptual model for effective directional emissivity for non isothermal surface," *IEEE Trans. Geosci. Remote Sens.*, vol. 37, no. 5, pp. 2508–2517, Sep. 1999.

[33] X. Li and J. Wang, "On the definition of effective emissivity of land surface at the scale of remote sensing pixels," *Chinese Sci. Bull.*, vol. 44, no. 15, pp. 1612–1617, Aug. 1999b.

[34] E. F. Vermote and D. P. Roy, "Land surface hot-spot observed by MODIS over Central Africa," *Int. J. Remote Sens.*, vol. 23, no. 11, pp. 2141–2143, Jun. 2002.

Huaguo Huang received the B.Sc. degree in forestry and the M.Sc. degree in forest management from Beijing Forestry University, Beijing, China, in 2001 and 2004, respectively, and the Ph.D. degree in quantitative remote sensing from the Institute of Remote Sensing Applications, Chinese Academy of Sciences, Beijing, in 2007.

He has been with the Forestry College, Beijing Forestry University, since 2007. He is currently an Associate Professor. His research interests include 3-D modeling of reflectance and thermal emission of land surfaces (vegetation in particular) and remote sensing applications in agriculture and forest environments.

Qinhuo Liu received the B.Sc. degree in hydrogeology and engineering geology from Southwest Jiaotong University, Chengdu, China, in 1988, and the M.Sc. degree in cartography and remote sensing and the Ph.D. degree in atmospheric physics from Peking University, Beijing, China, in 1994 and 1997, respectively.

He visited INRA of France, in 1998, Boston University in 1999, and the University of Maryland in 2003 as a Visiting Scholar. He has been with Institute of Remote Sensing Applications (IRSA), Chinese Academy of Sciences, Beijing, since 1997. He is currently a Professor, Deputy Director of the State Key Laboratory of Remote Sensing Science, IRSA, Chinese Academy of Sciences. His research interests include radiation transfer model of land surface, quantitative remote sensing inversion, assimilation and applications.

Wenhan Qin received the B.S. degree in meteorology from the Nanjing Institute of Meteorology and Graduate School, Nanjing, China, in 1983, the M.S. degree in meteorology from the University of Science and Technology of China in 1986, and the Ph.D. degree in geoscience and remote sensing from the Graduate School, University of Science and Technology of China, in 1992.

He was a Post-Doctoral Fellow with the Department of Computer Science, Wayne State University. from 1993 to 1995. During 1996 to 1999, he was with Code 923, NASA Goddard Space Flight Center (GSFC/NASA), Greenbelt, MD, as a Remote Sensing Scientist associated with the Department of Geography, University of Maryland at College Park, on 3-D scene simulation development and applications in remote sensing and ecological studies. Since 1999, he has been with Code 916 (now called 613.3), GSFC/NASA, as a Staff Scientist, and Senior Staff Scientist (since 2001) of SSAI on satellite remote sensing of atmospheric properties such as ozone and aerosols.